SAND2016-7155J

Dynamics of Crowding-Induced Mixing in Phase Separated Lipid Bilayers

Wade F. Zeno[‡], Kaitlin E. Johnson[‡], Darryl Y. Sasaki[¶], Subhash H. Risbud[†], and Marjorie L. Longo*[‡]

[‡]Department of Chemical Engineering, University of California Davis, Davis, California 95616, United States

[¶]Sandia National Laboratories, P.O. Box 969, Livermore, California 94551, United States

[†]Department of Materials Science and Engineering, University of California Davis, Davis, California 95616, United States

ABSTRACT

We use fluorescence microscopy to examine the dynamics of the crowding induced mixing transition of liquid ordered (L_o)-liquid disordered (L_d) phase separated lipid bilayers when the following particles of increasing size bind to either the L_o or L_d phase: Ubiquitin, green fluorescent protein (GFP), and nanolipoprotein particles of two diameters (NLPs). These proteinaceous particles contained histidine-tags, which were phase targeted by binding to iminodiacetic acid (IDA) head groups, via a Cu^{2+} chelating mechanism, of lipids that specifically partition into either the L_o phase or L_d phase. The degree of steric pressure was controlled by varying the size of the bound particle (10-240 kDa) and the amount of binding sites present (i.e. DPIDA concentrations of 9 and 12 mol%) in the supported multibilayer platform used here. We develop a mass transfer-based diffusional model to analyze the observed L_o phase domain dissolution that, along with visual observations and activation energy calculations, provides insight into the sequence of events in crowding induced mixing. Our results indicate that the

degree of steric pressure and target phase influence not only the efficacy of steric-pressure induced mixing, but the rate and controlling mechanism for which it occurs.

INTRODUCTION

In aqueous environments, phospholipids self-assemble to form bilayers that can exist in either a solid or liquid phase.[1] Structure of the head group (i.e. size and charge), structure of the carbon tails (i.e. length and degrees of unsaturation), and temperature are several of the properties and conditions that determine whether a solid or liquid phase is formed.[1b, 2] When an appropriate amount of cholesterol is added to a binary solid-liquid phospholipid mixture, the solid and liquid phases become liquid-ordered (L_o) and liquid-disordered (L_d) phases, respectively.[1] Fluorescent probes and functionalized lipids are capable of selectively partitioning into either of these coexisting, immiscible phases due to their distinct compositions.[3] The contrast from fluorescent probe partitioning allows for visualization of phase separation via fluorescence microscopy, while functionalized lipids can allow for targeting binding of proteins to specific phases. This type of phenomenon has been of interest for development of a variety of biological materials, such as high-density arrays, microfluidic networks, and biosensors.[4] Tethering of proteins to bilayers via functionalized lipids has been previously achieved by several mechanisms, such as disulfide bonds, single-stranded DNA linkages, and biotinylation.[5] Another mechanism – the method of interest for the work presented here – is metal chelation.[6] Lipid head groups functionalized with iminodiacetic acid (IDA) are capable of coordinating divalent transition metals (e.g. Zn^{2+}, Ni^{2+}, Cu^{2+}) through four coordination sites, leaving the two remaining sites exposed.[7] Poly-histidine tags that are covalently attached to proteins of interest are then able to bind to these exposed sites. IDA membranes also exhibit reversibility after EDTA is added to the

system, as EDTA sequesters metal ions, causing proteins to become unbound.[8]

Dipalmitoyl iminodiaceticacid (DPIDA) and dioleoyl iminodiaceticacid (DOIDA) are two IDA-functionalized lipids that have been used for phase targeting of histidine-tagged proteins. DPIDA has been demonstrated to partition into dipalmitoyl phosphocholine (DPPC)-rich L_o phase, while DOIDA partitions into dioleoyl phosphocholine (DOPC)-rich L_d phase when both phases are present in a bilayer.[9] This partitioning is due to similarities in carbon tail structures, degree of unsaturation and length. Phase-specific binding of histidine tagged proteins to DPIDA and DOIDA in the presence of $CuCl_2$ has been extensively examined by Sasaki and coworkers.[8a, 9-10] Histidine-tagged green fluorescent protein (GFP) was often used for studying targeted binding. When targeting DPIDA, GFP's fluorescence served as a visual indicator of binding to the L_o phase in L_o-L_d phase separated unilamellar vesicles (GUVs). GUVs exhibited significant changes in shape and morphology, such as membrane bending and tubule formation. This was attributed to protein binding localized to the L_o domains, which resulted in crowding in the headgroup region and induced local curvature. This was most often observed when diphytanoyl phosphocholine (DPhPC) was incorporated into GUVs.

Similarly, crowding induced changes in L_o-L_d phase separation in GUVs containing DPPC, DOPC, and cholesterol as the main constituents was examined by Scheve *et al.*[11] Targeting and binding of histidine-tagged Ubiquitin, GFP, and Transferrin to the L_o phase was achieved via incorporation of DPIDA. Rather than membrane bending and tubule formation, the percentage of GUVs which were phase separated decreased, which was attributed to mixing of the L_o and L_d phase lipids. This behavior was attributed to the large steric pressure localized to the L_o domains by the L_o phase targeted binding. There was also an obvious trend linking protein size to ability to induce mixing measured by the percentage of mixed GUVs. Phase separated lipid bilayers

have an inherent free energy of mixing (ΔG_{mix}),[12] thus Scheve *et al.* developed an empirical thermodynamic model to compare enthalpy of mixing to steric pressure exerted by bound proteins. Our previous work expanded upon the work of Scheve *et al*. to develop and experimentally test a first principles thermodynamic model that more universally describes mixing behavior and is capable of being used for a wide variety of lipid compositions.[13] The model consisted of a Boltzmann distribution that was applied to mixing within GUV populations (i.e. percentage of mixed and unmixed GUVs). It also incorporated the steric-pressure contribution to free energy via the Carnahan-Starling equation of state. Values for ΔG_{mix} were determined for various lipid compositions; its value decreased as a critical/mixing composition was approached, thus validating the thermodynamic model. Similarly to Scheve *et al.*, we reported an in increase in mixing efficacy as the size of the particle binding to the L_o phase of the GUV increased. We also qualitatively investigated L_d phase targeting in GUVs via DOIDA incorporation and L_o phase targeting in planar lipid multibilayers (MBLs) via DPIDA incorporation. In both instances mixing was observed at elevated IDA lipid concentration. Though the initial phase-separated and final mixed states were analyzed, we made only a preliminary qualitative attempt to observe the kinetics and dynamics of the crowding induced mixing process in one MBL sample.

In this present work, we utilize fluorescence microscopy to quantitatively examine the time-dependent crowding induced mixing of L_o-L_d phase separated lipid bilayers. The process was observed on supported multibilayers consisting of DOPC/DPPC/cholesterol and DPIDA for L_o targeting or DOIDA for L_d targetting. Multibilayers remain associated with a flat surface throughout the process of exchange of buffers yet distanced enough to be decoupled from strong interaction with the substrate, making it easy to follow the dynamics of individual domains over

relatively long periods of time. We vary the steric pressure by varying the size and molecular weight of the histidine-tagged crowding agent and the surface density of the target lipid DPIDA. Histidine-tagged Ubiquitin (2.5 nm diameter, 10 kDa) and GFP (3.6 nm diameter, 28 kDa) were used. In addition to this, two different sized populations of histidine-tagged nanolipoprotein particles (NLPs) were used. NLPs are self-assembled particles consisting of phospholipids and proteins. Specifically, they are composed of a lipid bilayer patch (~100-200 lipids) with two parallel, amphiphilic membrane scaffold proteins (MSPs) belted around the outer periphery, shielding the exposed carbon lipid tails. NLPs are discoidal in shape with a thickness of 5 nm (i.e. the thickness of a lipid bilayer), and a diameter that can vary on the order of 10-20 nm.[14] The diameter of an NLP population is controlled by the length of the MSP.[14-15] Histidine-tagged MSPs of various lengths are commercially available.[16] MSP1 (25 kDa) and MSP3 (33 kDa) were used to synthesize NLP1 (9 nm diameter, 140 kDa) and NLP3 (14 nm diameter, 240 kDa). Histidine tagged NLPs are particularly useful for this work because of their large size scale and size tuneability through our choice of the scaffold protein. Our previous work validated the use of NLPs as model crowding agents.[13] Here we show that particle size and target phase not only influences the efficacy of steric-pressure induced mixing, but the rate and controlling mechanism at which it occurs. We develop a mass transfer-based diffusional model that, along with visual observations and activation energy calculations, provides insight to crowding-induced mixing mechanisms.

MATERIALS AND METHODS

Materials. Lyophilized, N-terminal histidine tagged Ubiquitin was purchased from Sigma-Aldrich, Inc. Green fluorescent protein (GFP) also containing an N-terminal histidine-tag was purchased from Thermo Fisher Scientific. Lyophilized Membrane Scaffold Proteins (MSPs),

which were used in the synthesis of NLPs, contained single N-terminal histidine tags and were purchased from Cube Biotech, Inc. The two types of MSP used were MSP1 (sold as MSP1D1-his, 217 amino acids, 25.3 kDa) and MSP3 (sold as MSP1E3D1-his, 277 amino acids, 32.6 kDa). Copper (II) chloride (≥ 99%), sodium cholate (≥ 99%), sodium chloride (≥ 99%), imidazole (≥ 99%), and methanol (≥ 99%) were purchased from Sigma-Aldrich, Inc. Chloroform was purchased from Fisher Scientific International, Inc. DPPC (1,2-dipalmitoyl-sn-glycero-3-phosphocholine), DOPC (1,2-dioleoyl-sn-glycero-3-phosphocholine), and cholesterol were purchased from Avanti Polar Lipids, Inc. Texas Red® DHPE (Texas Red® 1,2,-dihexadecanoyl-sn-glycero-3-phosphoethanolamine) and Oregon Green® 488 DHPE (Oregon Green® 488 1,2,-dihexadecanoyl-sn-glycero-3-phosphoethanolamine) were purchased in lyophilized states from Thermo Fisher Scientific. DPIDA[9] (1,2-dipalmitoyl-sn-glycero-triethyleneoxy-iminodiacetic acid) and DOIDA[17] (1,2-dioleoyl-sn-glycero-3-triethylenoxy-iminodiacetic acid) were synthesized according to previously reported protocols. Tris(hydroxymethyl)aminomethane (MB Grade) and hydrochloric acid (12.1 N) were purchased from USB Corporation and Fisher Scientific International, Inc., respectively. Ni-NTA agarose was purchased from 5 PRIME, Inc. All water used in the work described was purified using a Barnstead Nanopure System (Barnstead Thermolyne, Dubuque, IA) with a minimum resistivity of 17.9 MΩ•cm.

Preparation of Ubiquitin, GFP, and NLPs. Lyophilized Ubiquitin was dissolved in Tris Buffer (20 mM Tris, 100 mM NaCl, pH 7.4) at a concentration of 1 mg/mL then purified using Ni-NTA resin as described previously with other histidine-tagged proteins.[18] Protein yield was measured using UV-Vis absorption at 280 nm, then aliquoted and stored at -20°C. GFP was dissolved in water at a concentration of 0.1 mg/mL, aliquoted, and frozen at -20°C. Ubiquitin and GFP aliquots were thawed prior to binding experiments. NLPs containing DOPC and either MSP1 or

MSP3 were synthesized exactly as previously described.[13] NLPs used for DPIDA binding experiments were doped with 0.1 mol% Oregon Green-DHPE, while NLPs used for DOIDA binding experiments were not. This was due to potential electrostatic repulsion between the Oregon Green-DHPE in NLPs and Texas-Red DHPE in the L_d region of MBLs.[13]

Lipid Multibilayer Binding and Imaging Experiments. Planar lipid multibilayers (MBLs) were prepared by a standard spin-coating technique as previously described.[13] Briefly, appropriate amounts of DOPC, DPPC, Cholesterol, DPIDA or DOIDA, and Texas Red-DHPE were combined, dried under nitrogen gas, and dissolved in a Hexane/Methanol solution (93 %v/v Hexane) at a concentration of 1.1 mg/mL total lipid. Samples were then spin-coated onto a 1 cm^2 mica substrate at 3000 RPM for 40 seconds and dried under vacuum for at least 2 hours.

Samples were enclosed within open-top wells consisting of 3D printed polylactic acid (PLA) squares adhered to polystyrene Petri dishes with vacuum grease. PLA squares had dimensions of 1.5 cm x 1.5 cm with a depth of 0.4 cm. Each well was hydrated in Tris Buffer (20 mM Tris, 100 mM NaCl, pH 7.4), heated to 55°C on a heating plate, and held there for at least 5 minutes before being removed and allowed to cool to room temperature. After cooling, excess buffer around the outer periphery of the PLA well was removed. Prior to imaging, each well contained supported MBLs on mica hydrated with 900 μL of Tris buffer. To each well, 6.8 μL of 16 mM $CuCl_2$ was then added. Afterward, concentrated stocks of Ubiquitin, GFP, NLP1, or NLP3 were added to their respective sample such that the final concentration was 0.2 μM. After mixing behavior was observed, 3.6 μL of 0.5 M EDTA was added to remove proteins and observe domain reformation.

Imaging was performed using a 60X water immersion lens on a Nikon TE400 fluorescence microscope. The microscope contained FITC and Texas Red filters (Chroma Technology,

Bellows Falls, VT). For visualization of GFP and Oregon Green-DHPE-containing NLPs, the FITC filter was used, while Texas Red Filters were used to visualize MBLs containing Texas Red-DHPE. Since Ubiquitin is non-fluorescent, it could not be visualized directly. With the concentrations of dye and protein used, no visual overlap was observed between the two filters (i.e. lipid domains could not be seen in the FITC filter and GFP/NLPs could not be seen in the Texas-Red Filter).

Data Processing and Numerical Methods. Microscope images of MBLs used in quantitative analysis for examining diffusion behavior were processed by converting 16-bit images to black/white binary pixelated images with ImageJ as shown in Fig. S3. The area fractions of the converted images were then determined using the "Analyze Particles" tool. Standard deviations of 4 quadrants within the microscope field of view were used to determine the error in Area Fraction for data points that were regressed. Processed images were regressed with Least Squares using the Runge-Kutta 4^{th} order method for numerical integration. The program for finding numerical solutions was written and performed in MATLAB. Errors in regressed parameters were determined by regressing parameters to the upper and lower ends of error bars from experimental data.

RESULTS

Dynamics of Steric Pressure-Induced Mixing by Binding to L_o Phase. We incubated histidine-tagged Ubiquitin (~10 kDa), GFP (~28 kDa), NLP1 (~140 kDa), or NLP3 (~240 kDa) with supported lipid multibilayers (MBLs) that contained two different concentrations of DPIDA, 12 mol% or 9 mol% in a 3:2 molar ratio of DOPC:(DPPC+DPIDA), 18 mole % cholesterol, and 0.01 mol % Texas Red-DHPE. These compositions display liquid ordered (L_o) -

liquid disordered (L_d) phase coexistence.[11] The DPIDA lipid partitions to the L_o phase and the histidine tags of proteins bind to the IDA headgroup in the presence of $CuCl_2$, thus targeting binding to the L_o phase.[20, 23] Texas Red-DHPE partitions strongly to the L_d phase such that the L_o phase domains appear dark by fluorescence microscopy as shown in Fig. 1A. Cohen-Simonsen and coworkers have shown that the L_o phase domains proximal to the substrate, are sub-microscopic, while those in subsequent bilayers coarsen quickly to form microscopic domains, as seen in Fig 1A. The domains observed here are in the second, and only other, bilayer distal to the substrate indicated by the lack of observation of any overlapping domains.

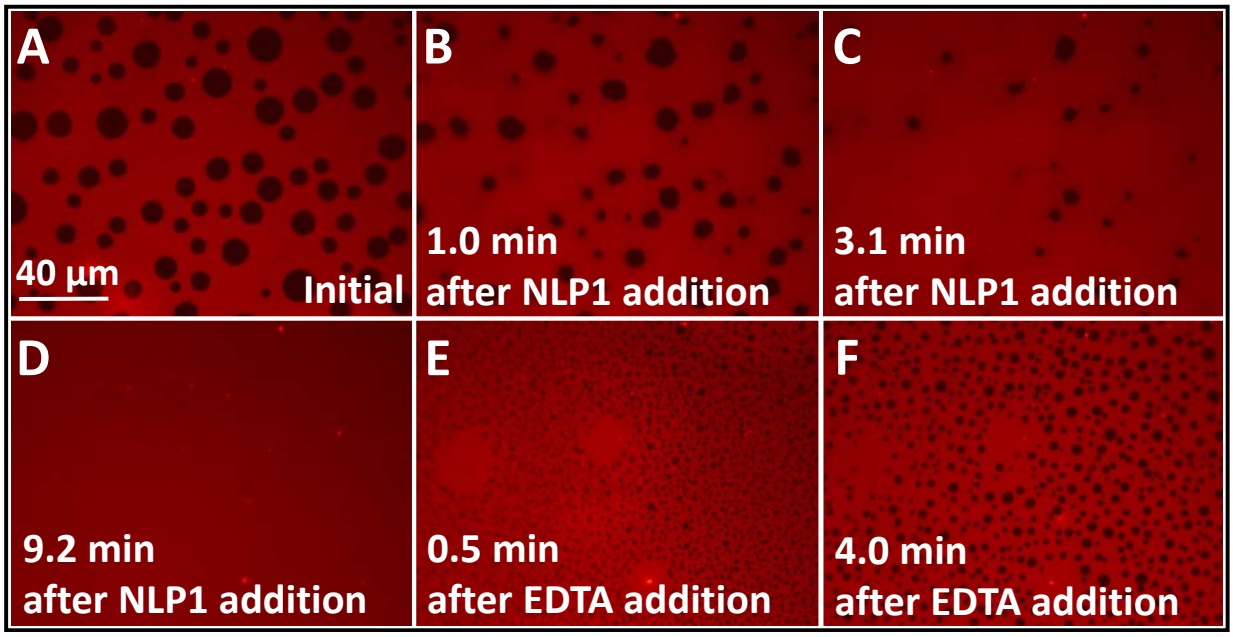

Figure 1: Dissolution of L_o phase domains in L_o-L_d phase separated multibilayers after addition of histidine tagged NLP1 (A-D), followed by removal of NLP1 with EDTA and L_o phase domain reappearance (E & F). The multibilayer composition was 49.9/20/12/18/0.1 mol% DOPC/DPPC/DPIDA/Cholesterol/Texas Red-DHPE.

We observed crowding-induced dissolution of the L_o domains of MBLs containing 12% DPIDA when incubated with histidine-tagged GFP, NLP1, and NLP3, as demonstrated by a decrease in

domain size as time progressed in Fig. 1A-D. We characterize the dynamics of this crowding-induced mixing mechanism by plotting the relative L_o domain Area Fractions (AF) vs. time, which decays exponentially to zero, apparently complete dissolution, in these cases as shown in Fig. 2A. The L_o domains bound by the smallest species, Ubiquitin, exhibited partial dissolution with a final relative AF of 0.87 ± 0.08, but no clear exponential decay (Fig. 2A). The L_o domains bound by GFP, NLP1, and NLP3, in order of smallest to largest, exhibited a final relative AF of zero within 9, 6, and 2 minutes, respectively. Immediately afterward, 2 mM EDTA was used to remove these bound proteins, resulting in the reappearance and growth of L_o domains as demonstrated in Fig 1D-F. In Fig. 2B, it can be seen that the relative AF returned to 80% of the original value for GFP and 90% for NLP1 and NLP3 within 1 minute after EDTA is added, indicating that the dissolution that we observe here is a reversible mixing transition. During all domain dissolution and domain growth, the vicinity close to the domains tended to have a granular appearance as shown clearly in Fig. 1B.

For MBLs containing 9% DPIDA, complete dissolution of the L_o domains was observed when incubated with NLP3, the largest species of the four (Fig. 2C). Incubation with NLP1 resulted in significant dissolution, with a residual relative AF of 0.06 ± 0.01 after completion. This final value did not change significantly over the final 5 minutes as seen with the data points in Fig. 2C. After addition of 2 mM EDTA, the relative AF for these two cases returned to 85-90% of their original value within a 1 minute time period, as shown in Fig. 2D. No significant change in relative AF was observed when incubating in the smaller species, Ubiquitin or GFP, over an 8-9 minute period as shown in Fig. 2C.

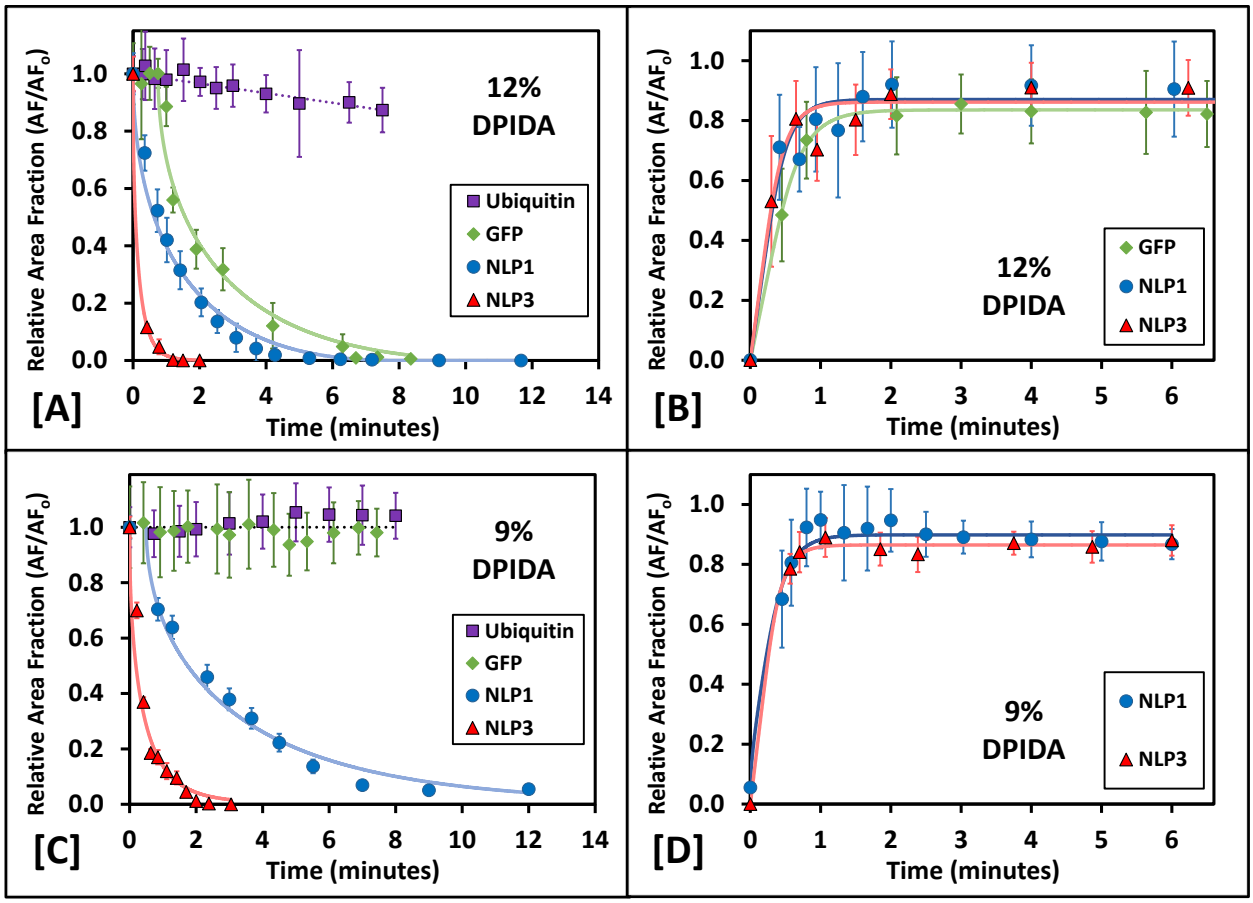

Figure 2: Changes in relative L_o domain area fraction with time after protein addition (A & C) and protein removal with EDTA (B & D) for multibilayers containing different amounts of DPIDA. Corresponding best fit curves are included. The multibilayer composition was 49.9/32/18/0.1 mol% DOPC/(DPPC+DPIDA)/Cholesterol/Texas Red-DHPE. Error bars are the propagated standard deviation of 4 different area fraction measurements.

Dissolution of L_o phase domains began immediately after NLP1 and NLP3 were added to phase-separated MBLs containing 12% DPIDA and when the larger of the two NLPs, NLP3, was added to phase-separated MBLS containing 9% DPIDA. However, for other samples, immediately after protein was added, smaller L_o domains were ejected from larger L_o domains, keeping the relative AF constant over the course of about 1 minute as demonstrated in Fig. 3A-B. These ejected domains were seen to grow by coalescence or Ostwald ripening as demonstrated in

Fig. 3B-C. Imaging of the bound NLP1 showed that the bound species were primarily located in the L_o phase (small and large green domains in Fig. 3C) during this initial period. After this initial period of domain break up, domains proceeded to dissolve, as demonstrated in Figs. 3D-F, for GFP or Ubiquitin binding to 12% DPIDA MBLs and NLP1 binding to 9% DPIDA MBLs. In the case of Ubiquitin binding to 12% DPIDA MBLs, domain dissolution took place so slowly that coalescence and Ostwald ripening were still observable phenomena during dissolution (see Fig. S4). Only the domain break-up was observed when GFP was incubated with 9% DPIDA MBLs. The small protein Ubiquitin imparted no observable change in relative AF or domain size to the 9% DPIDA MBLs.

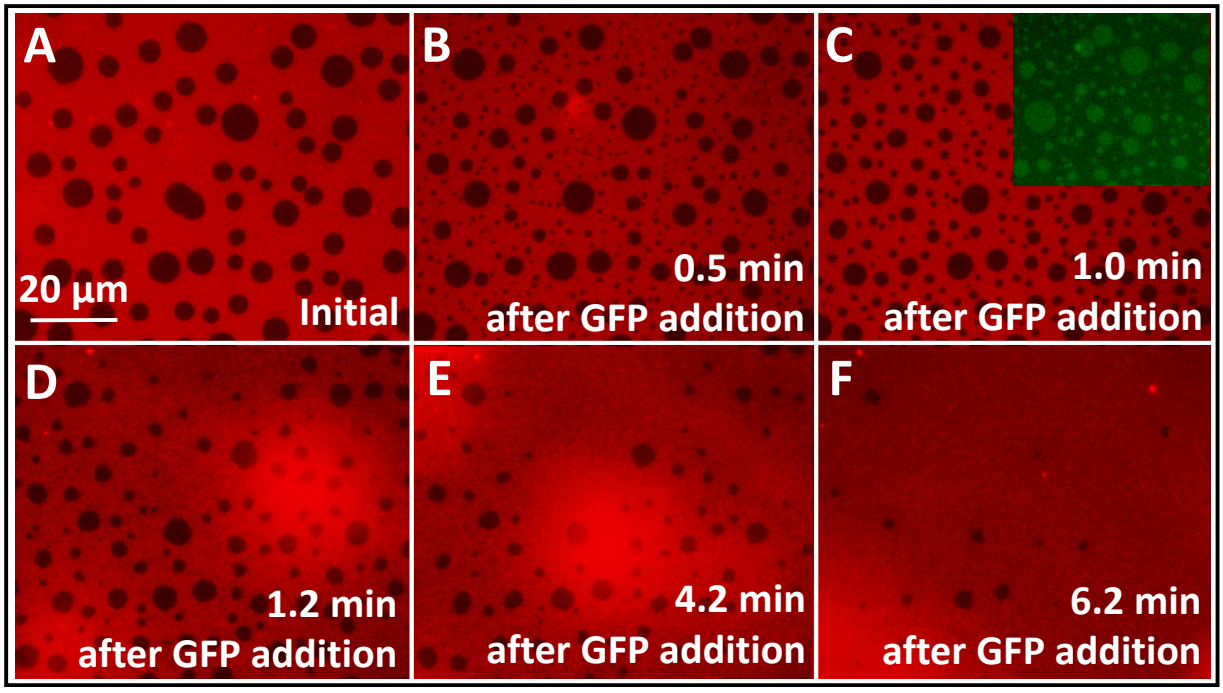

Figure 3: Break-up by ejection of small L_o phase domains in L_o-L_d phase separated multibilayers after addition of histidine tagged NLP1 (A-B) followed by and coalescence/Ostwald ripening (B-C) and dissolution of the L_o phase domains (D-F). The inset in (C) depicts protein binding visualized via the FITC filter. The multibilayer composition was 49.9/20/12/18/0.1 mol% DOPC/DPPC/DPIDA/Cholesterol/Texas Red-DHPE.

Modeling of Steric Pressure-Induced L_o Domain Dissolution and Curve Fitting.

The dissolution of liquid ordered domains was modelled using the time dependent diffusion equation, as shown in equation 1, where D corresponds to the diffusivity of the lipids ($\mu m^2/s$). The idealized system is illustrated in Fig. 4, where L_o domains are shown starting with an initial radius of R_o that decreases in size over time. The region of mass transfer (r) corresponds to the annulus between the outer periphery of a domain (R(t)) and the average midpoint to neighboring domains (R_b). R_o correspond the average initial domain radius. The initial and boundary conditions for equation 1 are listed in equations 1a-c. At initial time, there is a non-zero concentration of L_o domain lipids in the annulus (C_1). The L_o domains are assumed to have constant, uniform concentrations of C_o. Since domain lipids diffuse outwardly towards the boundaries, the net flux across boundaries midway between domains is equal to zero.

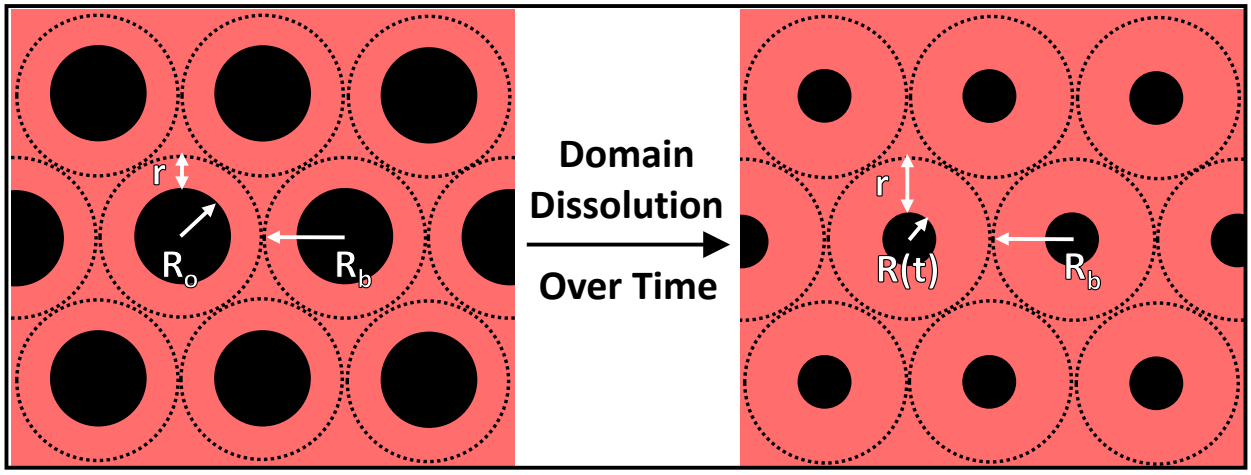

Figure 4: Schematic of idealized liquid ordered phase domain dissolution used in model. At initial time, domains have an average radius of R_o. As time progresses, average domain radius R(t) decreases. Diffusion occurs in an annular region with average thickness of r increasing with time.

$$\frac{\partial C(t,r)}{\partial t} = D\nabla^2 C(t,r),\ t \in [0,\infty],\ r \in [R(t), R_b] \quad (1)$$

$$C(0,r) = C_1 \quad (1a)$$

$$C(t,R) = C_o \quad (1b)$$

$$\left.\frac{\partial C}{\partial r}\right|_{r=R_b} = 0 \quad (1c)$$

Equation 1 was solved analytically using separation of variables and a 1-dimenstional Cartesian Laplacian, rather than cylindrical, because an analytical solution in cylindrical coordinates with the given boundary conditions is difficult to obtain. By looking at numerical solutions to both Cartesian and Cylindrical coordinates, it was found that this is a reasonable approximation in the region of the concentration profile close to the domain boundary (i.e. the region of interest for this analysis). The concentration profile is shown in equation 2, where the eigenvalues of the Sturm-Liouville problem are defined in equation 2a. (See Supporting Information for detailed derivation)

$$C(t,r) \approx C_o + 2C_o\left(\frac{C_1}{C_o} - 1\right)\sum_{n=0}^{\infty}\left[e^{-\frac{\lambda_n^2 Dt}{(R_b-R)^2}}\sin\left(\frac{\lambda_n(r-R)}{R_b-R}\right)\left(\frac{1}{\lambda_n}\right)\right] \quad (2)$$

$$\lambda_n = \pi\left(\frac{2n+1}{2}\right) \quad (2a)$$

An interfacial mass balance was performed around the outer surface of a domain. The time dependent rate of change of mass within a domain is equal to the flux of lipids out of the domain multiplied by the domain perimeter. The ordinary differential equation for this balance is shown in equation 3, with an initial condition of the radius equal to R_o (equation 3a).

$$\frac{d}{dt}[C_o\pi R(t)^2] = D\left.\frac{\partial C}{\partial r}\right|_{r=R(t)}[2\pi R(t)] \quad (3)$$

$$R(0) = R_o \quad (3a)$$

By algebraically manipulating equation 3 and substituting in equation 2 for C, equation 4 for $\frac{dR}{dt}$

was obtained and solved numerically. The average relative area (R/R_o) of domains relative corresponds to the area fraction (AF/AF_o) as shown in equation 5.

$$\frac{dR}{dt} = \frac{2D\left(\frac{C_1}{C_o}-1\right)}{(R_b-R)} \sum_{n=0}^{\infty} \left[e^{-\frac{\lambda_n^2 Dt}{(R_b-R)^2}} \right] \qquad (4)$$

$$\frac{AF}{AF_o} = \left(\frac{R}{R_o}\right)^2 \qquad (5)$$

The data for AF/AF_o vs. time in Fig. 2A and Fig. 2C were regressed using equations 4 and 5 by the least squares method. The variable parameters for this regression were D and C_1/C_o. For modelling the reversed process (i.e. protein removal and domain reformation), equations 4 and 5 were used with a negative sign on the right hand sign of equation 4, as the diffusive flux is now into the domain rather than out of it. The value of AF_o from the mixing model was used for its corresponding reversal model.

As shown in Fig. 2, regression curves are in agreement with experimental data, for all samples. Meaningful regression curves could not be generated in the cases where there was no dissolution or where the change in relative AF was minor. Diffusion coefficients (D) obtained from dissolution data appear to be correlated to the size of the bound protein or NLP, as seen in Table 1. D increased from ~0.02 $\mu m^2/s$ to an at least an order of magnitude higher as particle size increased from 10 nm^2 (GFP) to 153 nm^2 (NLP3). It is also worth noting that bound NLP3 imparted a higher D value in 12% DPIDA in comparison to 9% DPIDA. Diffusion coefficients obtained by demixing data shown in Table 1 were of magnitude ~0.3 $\mu m^2/s$, and relatively similar for all samples, as expected, since protein was no longer bound.

Table 1: Regressed values for diffusion coefficients (D) using equations 4 and 5.

	Crowding Particle	**Mixing Diffusion Coefficient (D) ($\mu m^2/s$)**	**Demixing Diffusion Coefficient (D) ($\mu m^2/s$)**

12% DPIDA	Ubiquitin	-	-
	GFP	0.02 ± 0.01	0.15 ± 0.06
	NLP1	0.06 ± 0.01	0.55 ± 0.20
	NLP3	0.79 ± 0.08	0.65 ± 0.22
9% DPIDA	Ubiquitin	-	-
	GFP	-	-
	NLP1	0.06 ± 0.01	0.62 ± 0.13
	NLP3	0.18 ± 0.05	0.31±0.07

Activation Energy Approximation for Steric Pressure-Induced L_o Domain Dissolution. The range of diffusion coefficients obtained from the dissolution data could indicate a transition from a kinetically limited process (slow dissolution) to a diffusion limited process (fast dissolution). The activation energy (E_A) associated with lipids transferring from a L_o domain to the surrounding L_d region was approximated using Arrhenius kinetics. Detailed calculations are provided in the Supporting Information. Briefly, relative rates of domain dissolution induced by GFP, NLP1, and NLP3 binding to 12% DPIDA MBLs were compared. Using the Arrhenius equation (equation 10), an activation energy cannot be calculated directly since there are 3 equations (an Arrhenius equation for each particle binding) and 4 unknowns (an Activation Energy for each particle binding and the Arrhenius pre-exponential factor A).

$$reaction\ rate\ \propto k = Ae^{-\frac{E_A}{k_B T}} \qquad (10)$$

By comparing regressed reaction rate constants (k) between two samples, a change in activation energy ΔE_A was determined. Dissolution time scales decreased as particle size increased (Fig. 2), indicating that E_A also decreased as particle size increased (i.e. reaction rate increased). MBLs bound with NLP1 exhibited a 0.1kT decrease in E_A relative to MBLs bound with GFP, whereas MBLs bound with NLP3 exhibited 1.8kT decrease in comparison to those bound with NLP1. Based on these values for ΔE_A, we were able to infer that E_A for a bilayer with no particles bound is on the order of 1-2kT (~ 4 to 8×10^{-21} Joules/lipid).

Determination of ΔG_{mix} from Steric Pressure-Induced L_o Domain Dissolution. The Boltzmann distribution, shown in equation 7, relates the free energy to the partitioning of lipids between two states (mixed and unmixed) at equilibrium.[19] For the system being examined, there are two contributions to the free energy; the inherent free energy of mixing (ΔG_{mix}) and the free energy associated with steric pressure (ΔG_p). The partition coefficient (K) is shown in equation 7 and defined in equation 8 as the ratio of unmixed lipids to mixed lipids at equilibrium. This result was obtained by performing a mass balance on a domain with initial and final equilibrium radii assuming a mixing zone exists. (See supporting information).

$$k_B T * \ln(K) = \Delta G_{mix} + \Delta G_p \qquad (7)$$

$$K = \frac{N_{unmixed}}{N_{mixed}} = \frac{\frac{1}{AF_o} - \left(1 - \frac{AF}{AF_o}\right)\left(\frac{1}{AF_o} - \frac{AF}{AF_o}\right)}{\left(1 - \frac{AF}{AF_o}\right)\left(\frac{1}{AF_o} - \frac{AF}{AF_o}\right)} \qquad (8)$$

Previously, we demonstrated that the steric pressure contribution to free energy can be determined by integrating the Carnahan-Starling equation state over the change in fractional surface coverage (η) of the binding species before and after complete mixing.[13] The initial surface coverage (η_i) and final surface coverage (η_f) were determined by knowing how much DPIDA is contained in the bilayer.[11, 13] Details of these calculations are provided in the Supporting Information. When this is applied to ΔG_p in equation 7, equation 9 is obtained. N_P and N_L correspond to the number of proteins and lipids in a given area of bilayer, respectively.

$$\Delta G_{mix} = k_B T * \ln(K) - \int_{\eta_i}^{\eta_f} \frac{N_p}{N_L} k_B T \left(\frac{1+\eta+\eta^2-\eta^3}{\eta[1-\eta]^3}\right) d\eta \qquad (9)$$

Use of equation 9 requires a final relative AF that is neither 0 nor 1. Two samples yielded values that satisfy this criteria; NLP1 bound to 9% DPIDA MBLs (0.06 $\pm$ 0.01) and Ubiquitin bound to 12% DPIDA MBLs (0.87 $\pm$ 0.08). Based on these AF values, ΔG_{mix} was determined to be $(1.0 \pm 0.5) * 10^{-20}$ Joules/Lipid for the former, and $(1.1 \pm 0.3) * 10^{-20}$ Joules/Lipid for the latter. These

values are on the same order of magnitude as those previously determined for this lipid composition in giant unilamellar vesicles (GUVs).[13]

Steric Pressure-Induced Membrane Remodeling by Binding to L_d Phase. Next, we incubated histidine-tagged NLP1 (~140 kDa) with lipid multibilayers (MBLs) of compositions that display liquid ordered (L_o) - liquid disordered (L_d) phase coexistence and contained 20 mol% DOIDA, 18 mole % cholesterol, .01% Texas Red-DHPE, and a 3:2 molar ratio of DOPC:(DPPC+DPIDA). The DOIDA lipid partitions to the L_d phase, therefore histidine tagged NLP1 binds primarily to the L_d domains rather than the L_o domains. As shown in Figs. 5A-C, binding of NLP1 to the L_d region resulted in a generally less circular appearance of the L_o domains, some of which appear to have coalesced. The relative AF of the domains had not perceptively changed. However, small, light L_d domains can be seen to appear inside the L_o domains after 1.5 minutes (Fig. 5C). This phenomena is similar to the break-up of the L_o phase observed previously for example in Fig. 3A-C. The L_d region also appeared to darken as time progressed. After addition of 2 mM EDTA (Figs. 5D-F), the L_d region became brighter and numerous small vesicles appeared on the edges of the L_o domains, as indicated by the white dots, and the domains took on a leaf-like shape as seen in Fig. 5D. In addition, holes formed in the L_d portion of the bilayer as illustrated by the irregularly shaped dark red patches. L_o domains proceeded to round-up and coalesce while avoiding contact with bilayer holes, while entrapping some L_d "subdomains" within the L_o domains (Fig. 5D-E).

When we waited longer before adding the EDTA, the L_d domains inside of the L_o domains appear to increase in density and finally form vesicles (see Fig. S5) rather than mixing with the L_o phase via dissolution. Therefore, the quantitative dissolution model could not be applied to these binding experiments. Wide-spread removal of the MBL through a process reminiscent of

surface folding was the next step (Data not shown). When EDTA was added no reversible effects were observed.

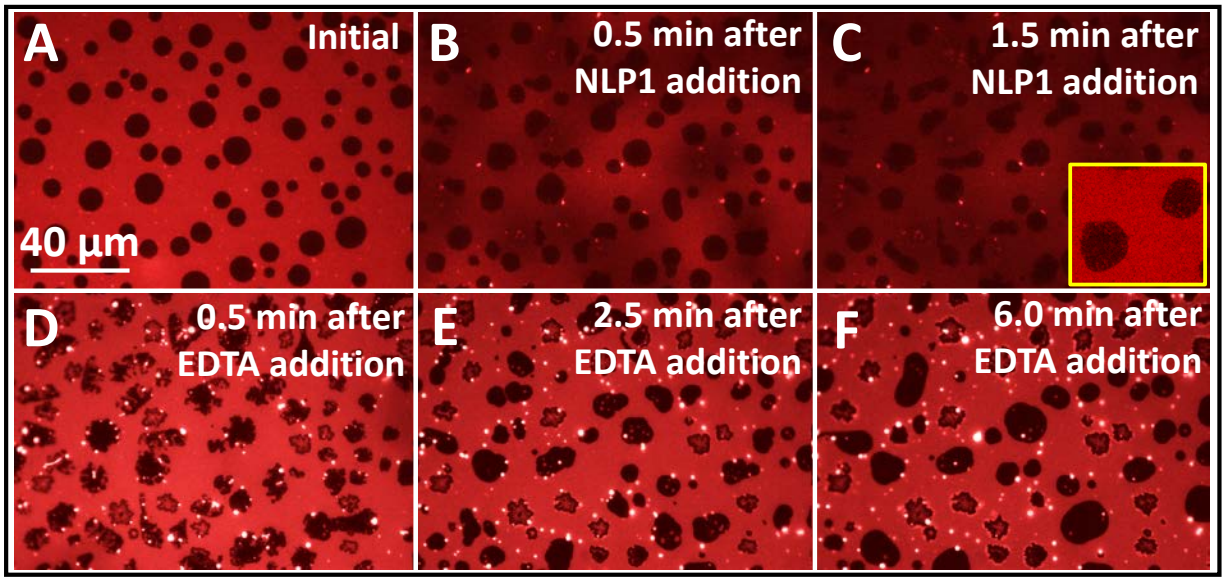

Figure 5: Morphological changes in L_o-L_d phase separated multibilayers after addition of histidine tagged NLP1 (A-C) followed by removal of NLP1 with EDTA that resulted in domain coalescence (D-F). Holes in the bilayer appear as dark red leafy figures. Enhanced visualization of L_d domains within L_o domains is depicted in (C) inset. The multibilayer composition was 29.9/32/20/18/0.1 mol% DOPC/DPPC/DOIDA/Cholesterol/Texas Red-DHPE.

The elongated appearance and lack of change in size of the domains was initially thought to be indicative of a gradual mixing process, akin to reversal of spinodal decomposition. To investigate this hypothesis, domain formation during cooling at this same lipid composition was observed as shown in Fig. 6. The domain formation is clearly indicative of nucleation and growth with the lipid composition used, thus the observed behavior is likely not related to spinodal decomposition.

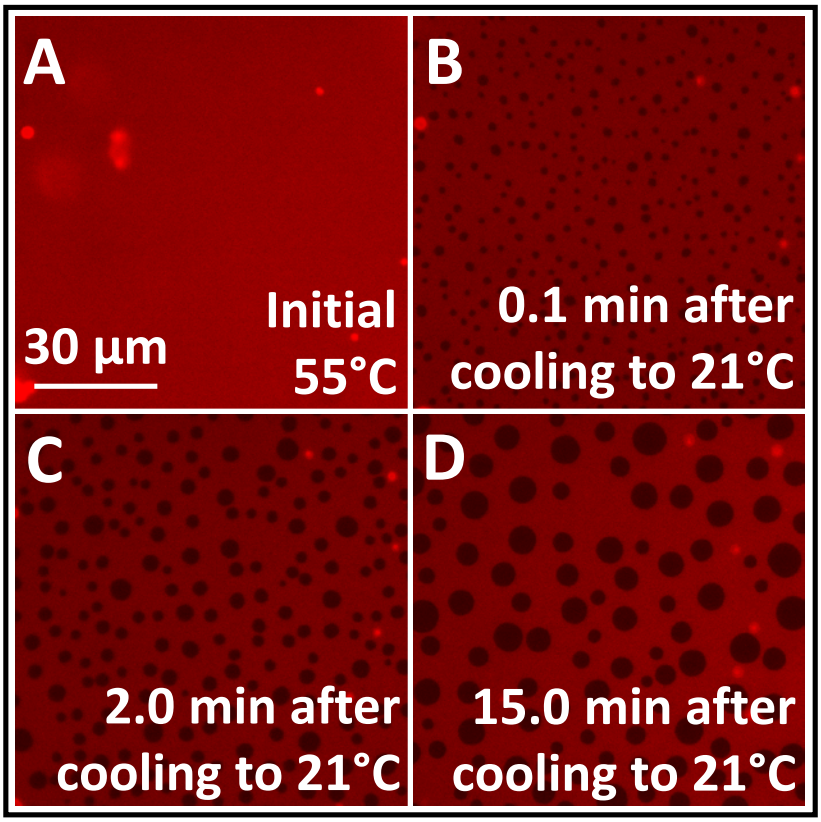

Figure 6: Nucleation and growth observed in MBLs containing 29.9/32/20/18/0.1 mol% DOPC/DPPC/DOIDA/Cholesterol/Texas Red-DHPE.

Steric Pressure-Induced Mixing by Binding to L_o Phase in the Spinodal Region. To further examine the possibility that the mechanism of the mixing process is coupled with the mechanism of domain formation (i.e. nucleation and growth vs. spinodal decomposition), we examined the targeted binding of NLP1 to L_o domains in MBLs with a composition consisting of a 1:1 DOPC:(DPPC+DPIDA) with 26 mol% Cholesterol and 0.1 mol% Texas Red-DHPE. The DPIDA concentration used was 14 mol%. In Fig. 7, it can be seen that this composition was in the spinodal region of the phase diagram indicated by the elongated interlaced domain shapes (Fig. 7B) during domain formation by cooling. After L_o domain formation and NLP1 addition to the system, domains were observed to undergo mixing via dissolution over the course of 3

minutes as illustrated in Figs. 8A-8D. Upon removal of the NLP1 with EDTA (Figs. 10E-10F), L_o domains reappeared and were elongated enough (Fig. 7C and 8E are comparable) to suggest recovery of growth in the spinodal region. These results indicate that during L_o targeted mixing of MBLs, the domains will undergo mixing via a dissolution mechanism rather than gradual spinodal-like mixing regardless of their compositional location on a phase diagram.

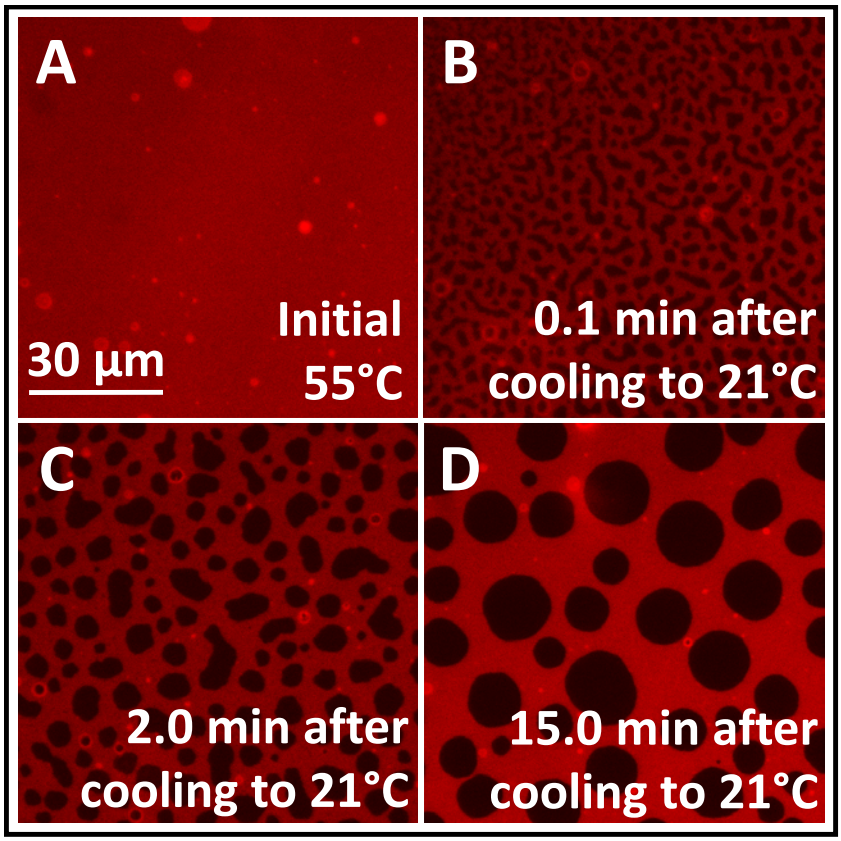

Figure 7: Formation of domains in the spinodal region of the phase diagram with MBLs containing 36.9/23/14/26/0.1 mol% DOPC/DPPC/DPIDA/Cholesterol/Texas Red-DHPE.

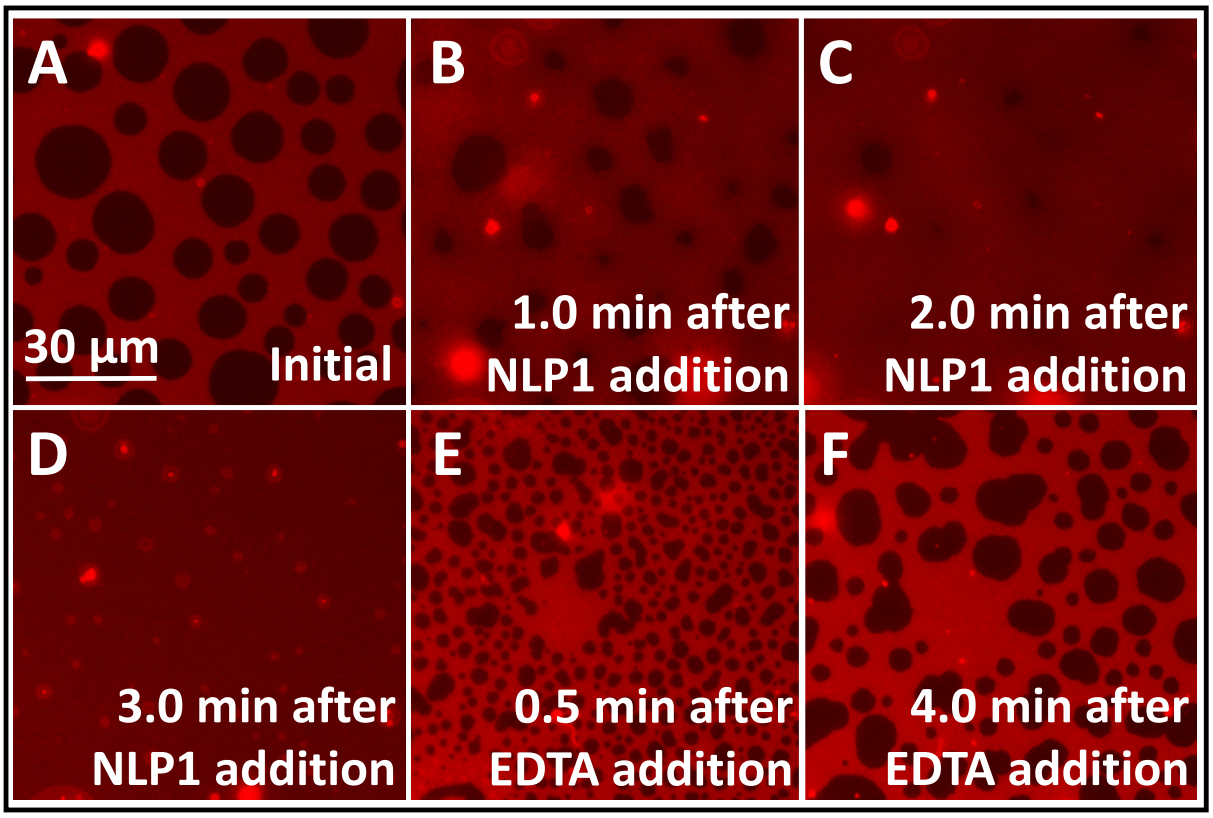

Figure 8 Dissolution of L_o domains by addition of NLP1 to L_o-L_d phase separated multibilayers (A-D) and reappearance of domains by spinodal decomposition after addition of 2 mM EDTA (E-F). MBLs contained 36.9/23/14/26/0.1 mol% DOPC/DPPC/DPIDA/Cholesterol/Texas Red-DHPE.

DISCUSSION

Crowding induced dissolution of L_o phase domains in L_o-L_d phase separated lipid bilayers appears to involve two sequential rate processes, the kinetic process of release of L_o phase clusters from the domains followed by diffusion of those clusters driven by a concentration gradient. Evidence includes the increase by almost 2 orders of magnitude in the diffusion coefficients calculated from the dissolution data as the steric pressure is increased by increasing the size of the bound protein or NLP. In comparison there is a relatively steady diffusion coefficient calculated from the time-dependent growth of domains after removal of the bound proteins or NLPs by EDTA. The variation in this apparent diffusion coefficient likely represents a transition from a slow kinetically limited dissolution process at low steric pressure, induced by a small bound protein such as GFP, to faster kinetics and thus a diffusion-limited process at high steric pressure, induced by a large bound particle such as NLP3. This could be explained by considering the mechanism of the kinetic process. The intermediate state is likely a thermal shape fluctuation of the domain boundary that results in pinching off of a small cluster of the target phase evidenced by the graininess, i.e. domains below ~0.5 μm in size, in the L_d regions surrounding domains as they dissolved. Such thermal fluctuations are normally of energy approximately kT.[19] As the size of the bound particle increases, the free energy contribution from steric pressure is increased. This corresponds to higher energy in the initial, phase-separated state. This relative increase in initial energy would result in a decrease of the energy barrier for the mixing process. Using Arrhenius kinetics, this corresponds to a faster rate of reaction, i.e. pinching off clusters, as steric pressure is increased. Thus this kinetic process is no longer limiting the dissolution rate. We calculated that the decrease in the activation energy would have to be at least 1.8 kT in agreement the energy scale of commonly occurring thermal shape fluctuations.

The plateau in diffusion coefficient values between 0.2 $\mu m^2/s$ and 0.8 $\mu m^2/s$ is additional evidence of dissolution (and regrowth) by lipid clusters vs individual lipids, as diffusivity generally varies inversely with size. Typical diffusion coefficients for lipids diffusing in an L_d phase are on the order of 1-10 $\mu m^2/s$.[20] The Saffman–Delbrück model is an appropriate model for calculating diffusion coefficients of species within lipid bilayers.[21] Using this model, it was calculated that lipid clusters consisting of 10^3-10^4 lipids result in an order of magnitude reduction of diffusion coefficient relative to that of a single lipid (see Supporting Information). Clusters of such small size would only appear as a change in texture (graininess) of the region around the dissolving or regrowing domains – consistent with what is observed. Such nanoscopic clusters are capable of dissolving or appearing rapidly through thermal compositional fluctuations which we postulate happened in the final stage of mixing by the highest free energy contributions from steric pressure (NLP3 bound to 9% and 12% DPIDA domains and NLP1 bound to 12% DPIDA domains) and first stage of regrowth by addition of EDTA.

We attempted to change the mechanism of crowding-induced mixing from dissolution (reversal of nucleation and growth) to gradual demixing (reversal of spinodal decomposition) by changing the membrane composition to one that is near a critical point. However, dissolution was still observed in the new composition when NLP1 bound to the L_o phase. This can be explained by considering that during domain formation, small composition fluctuations in the spinodal region of the phase diagram exhibit negative free energies, thus making them favorable. This allows for the gradual formation of interlaced domains as typically seen in spinodal decomposition that gradually change in composition. However, when the process is reversed (i.e. steric pressure induced mixing), the composition fluctuations now exhibit positive free energies and are unfavorable. This eliminates the gradual mixing of the two phases as a process. It becomes more

favorable to maintain the initial compositions of the L_d and L_o phases during mixing process as this minimizes composition fluctuations. The dissolution process occurring via lipid clusters rather than individual lipids is especially favorable, since they help to maintain domain composition. These can finally break up through large compositional fluctuations similar to reversal of nucleation.

When the magnitude of the free energy contribution from the crowding pressure ($\Delta G_{p,}$ a negative number) is less than the free energy change from mixing (ΔG_{mix}), the addition of ΔG_p to ΔG_{mix} gives a new apparent ΔG_{mix}. This smaller ΔG_{mix} will, in turn, be associated with a new equilibrium composition of each phase with more similar compositions closer to a critical point. A possible mechanism to achieve this new equilibrium was observed here in the break-up of the target phase by release of micron-scale domains from the target phase. The release of small domains of the target phase was followed by Ostwald ripening and coalescence as these may serve as mechanisms to move to a new equilibrium composition of each phase by slightly readjusting the composition of each phase without significantly changing the relative area fraction of each phase. In case the new equilibrium compositions nearly merge, i.e. near a critical point, the line tension is extremely low which may stabilize submicroscopic domains with new equilibrium compositions.[22] This might be mistaken as complete mixing when in fact nanoscopic domains still exist. This might explain the apparent observation of complete dissolution of L_o domains in MBLs containing 12% DPIDA when bound by GFP, as this was not expected. The calculated free energy contribution from steric pressure (ΔG_p) for GFP binding to 12 mol% DPIDA MBLs was -5.5×10^{-21} Joules/Lipid, as determined from the integral term in equation 9. The magnitude of ΔG_p is smaller than ΔG_{mix} determined to be roughly $(1.0 \pm 0.5) \times 10^{-20}$ Joules/Lipid.

When targeting the crowding agent, NLP1, to the L_d phase, membrane shape changes such as vesiculation and hole formation, played a major role in the drive toward equilibrium making it difficult to study mixing. Although we did some evidence of lipid mixing, i.e. the appearance of micron-scale L_d domains in the L_o phase domains. It is interesting that a similar experiment resulted in complete mixing of approximately 80% of the population of GUVs in our previous work.[13] This could be accounted for by a difference in tension of the bilayers used in these two studies. MBLs are presumably free of any osmotic gradients that would create tension to smooth out membrane bending. The GUVs in our previous study were placed in a slightly hypotonic solution that creates enough tension to prevent excessive vesiculation.

CONCLUSIONS

We examined the lipid mixing and demixing dynamics in L_o-L_d phase separated supported lipid multibilayers induced by steric pressure from phase targeted binding of histidine-tagged proteins and molecular assemblies of various sizes. When targeting the L_o phase by inclusion of DPIDA, mixing by the process of L_o domain dissolution was determined to be a two-step reaction-diffusion process. Dissolution was reaction-limited and slow when the steric pressure was low and diffusion-limited and fast when steric pressure was sufficiently high. Visual observation and the scale of the diffusion coefficients, determined through mass transfer analysis of the data, indicate that L_o domains appeared to break up and dissolve into the neighboring phase via ejection of sub-microscopic clusters and/or micron-scale domains rather than individual lipids. Therefore, the initial reaction consisted of an initial release of lipid clusters from L_o domains via shape fluctuations of the domain perimeter that we determined were of energetic order kT. This was followed by diffusion of lipid clusters via a concentration gradient in the L_d region. Reversibility was exhibited in all instances where domains appeared to completely or nearly

completely dissolve. These results were obtained by targeting L_o domains that formed in the nucleation/growth region of the phase diagram. For L_o domains formed in the spinodal region of the phase diagram, L_o domains mixed in a manner nearly identical to the dissolution observed in the nucleation/growth region as demanded by the curvature of the mixing energy with respect to composition. Moreover, using theory we previously derived, we were able to calculate values of ΔG_{mix} for multibilayers that are in agreement with our previously reported values for GUVs using similar compositions.

In addition to L_o domain targeting and dissolution, we qualitatively examined L_d region targeting in MBLs using DOIDA. We found that the overall mixing process induced by steric pressure from the L_d phase is inherently more complex and differs from what was observed with L_o targeting, as the L_d phase is more prone to deformation and shape fluctuations out of the two-dimensional MBL plane. However, similarities to L_o targeting were observed as the L_d phase sought to alleviate steric pressure by ejecting micron-scale L_d phase domains into the L_o domains.

SUPPORTING INFORMATION

The Supporting Information is available free of charge on the ACS Publications website.

Detailed derivations, image processing, additional figures and tables.

ACKNOWLEDGMENTS

MLL, SHR, and WFZ acknowledge partial support from the National Science Foundation under award number DMR- 1500275. WFZ was partially supported by Grant Number T32-GM008799 from NIGMS-NIH. SHR also acknowledges partial support derived from his Blacutt-

Underwood Endowed Chair funds. DYS was supported by the US Department of Energy, Office of Basic Energy Sciences, Division of Materials Science and Engineering. Sandia National Laboratories is a multi-program laboratory managed and operated by Sandia Corporation, a wholly owned subsidiary of Lockheed Martin Corporation, for the U.S. Department of Energy's National Nuclear Security Administration under contract DE-AC04-94AL85000.

REFERENCES

1. (a) Marsh, D., Cholesterol-induced fluid membrane domains: a compendium of lipid-raft ternary phase diagrams. *Biochim. Biophys. Acta* **2009,** *1788* (10), 2114-2123; (b) Veatch, S. L.; Keller, S. L., Seeing spots: complex phase behavior in simple membranes. *Biochim. Biophys. Acta* **2005,** *1746* (3), 172-185; (c) Juhasz, J.; Sharom, F. J.; Davis, J. H., Quantitative characterization of coexisting phases in DOPC/DPPC/cholesterol mixtures: comparing confocal fluorescence microscopy and deuterium nuclear magnetic resonance. *Biochim. Biophys. Acta* **2009,** *1788* (12), 2541-2552; (d) Lingwood, D.; Simons, K., Lipid rafts as a membrane-organizing principle. *Science (Washington, DC, U.S.)* **2010,** *327* (5961), 46-50.
2. Rawicz, W.; Olbrich, K. C.; McIntosh, T.; Needham, D.; Evans, E., Effect of chain length and unsaturation on elasticity of lipid bilayers. *Biophys. J.* **2000,** *79* (1), 328-339.
3. (a) Juhasz, J.; Davis, J. H.; Sharom, F. J., Fluorescent probe partitioning in GUVs of binary phospholipid mixtures: Implications for interpreting phase behavior. *Biochim. Biophys. Acta* **2010,** *1818* (1), 19-26; (b) Momin, N.; Lee, S.; Gadok, A.; Busch, D.; Bachand, G.; Hayden, C.; Stachowiak, J.; Sasaki, D. Y., Designing lipids for selective partitioning into liquid ordered membrane domains. *Soft Matter* **2015,** *11* (16), 3241-3250.
4. (a) Bally, M.; Bailey, K.; Sugihara, K.; Grieshaber, D.; Voros, J.; Stadler, B., Liposome and lipid bilayer arrays towards biosensing applicaitons. *Small* **2010,** *6* (22), 2481-2497; (b) Cornell, B. A.; Breach-Maksvytis, V. L. B.; King, L. G.; Osman, P. D. J.; Raguse, B.; Weieczorek, L.; Pace, R. J., A biosensor that uses ion channel switches. *Nature (London, U.K.)* **1997,** *387*, 580-582; (c) Stelzle, M.; Weissmüller, G.; Sackmann, E., On the application of supported bilayers as receptive layers for biosensors with electrical detection. *J. Phys. Chem.* **1993,** *97* (12), 2974-2981; (d) Ogunyankin, M. O.; Huber, D. L.; Sasaki, D. Y.; Longo, M. L., Nanoscale Patterning of Membrane-Bound Proteins Formed through Curvature-Induced Partitioning of Phase-Specific Receptor Lipids. *Langmuir* **2013,** *29* (20), 6109-6115; (e) Karlsson, M.; Sott, K.; Cans, A. S.; Karlsson, A.; Karlsson, R.; Orwar, O., Micropipette-assisted formation of microscopic networks for unilamellar lipid bilayer nanotubes and containers. *Langmuir : the ACS journal of surfaces and colloids* **2001,** *17* (22), 6754-6758.
5. (a) Seitz, M.; Wong, J. Y.; Park, C. K.; Alcantar, N. A.; Israelachvili, J., Formation of tethered supported bilayers via membrane-inserting lipids. *Thin Solid Films* **1998,** *327*, 767-771; (b) Svedhem, S.; Pfeiffer, I.; Larsson, C.; Wingren, C.; Borrebaeck, C.; Hook, F., Patterns of DNA-labeled and scFv-antibody-carrying lipid vesicles directed by material-specific immobilization of DNA and supported lipid bilayer formation on Au/SiO_2 template. *ChemBioChem* **2003,** *4* (4), 339-343; (c) Darst, S. A.; Ahlers, M.; Meller, P. H.; Kubalek, E. W.; Blankenburg, R.; Ribi, H. O.; Ringsdorf, H.; Kornberg, R. D., 2-Dimensional crystals of strepavidin on biotinylated lipid bilayers and their interactions with biotinylated macromolecules. *Biophys. J.* **1991,** *59* (2), 387-396.

6. Nye, J. A.; Groves, J. T., Kinetic control of histidine-tagged protein surface density on supported lipid bilayers *Langmuir : the ACS journal of surfaces and colloids* **2008,** *24* (8), 4145-4149.
7. Bornhorst, J. A.; Falke, J. J., Purifcation of proteins using polyhistidine affinity tags. *Methods Enzymol.* **2000,** *326*, 245.
8. (a) Hayden, C. C.; Hwang, J. S.; Abate, E. A.; Kent, M. S.; Sasaki, D. Y., Directed formation of lipid membrane microdomains as high affinity sites for His-tagged proteins. *J. Am. Chem. Soc.* **2009,** *131* (25), 8728-8729; (b) Ng, K.; Pack, D. W.; Sasaki, D. Y.; Arnold, F. H., Engineering protein-lipid interactions: targeting of histidine-tagged proteins to metal-chelating lipid monolayers. *Langmuir : the ACS journal of surfaces and colloids* **1995,** *11* (10), 4048-4055.
9. Stachowiak, J. C.; Hayden, C. C.; Sanchez, M. A. A.; Wang, J.; Bunker, B. C.; Voigt, J. A.; Sasaki, D. Y., Targeting Proteins to Liquid-Ordered Domains in Lipid Membranes. *Langmuir : the ACS journal of surfaces and colloids* **2010,** *27* (4), 1457-1462.
10. (a) Stachowiak, J. C.; Hayden, C. C.; Sasaki, D. Y., Steric confinement of proteins on lipid membranes can drive curvature and tubulation. *Proc. Natl. Acad. Sci. U.S.A.* **2010,** *107* (17), 7781-7786; (b) Stachowiak, J. C.; Schmid, E. M.; Ryan, C. J.; Ann, H. S.; Sasaki, D. Y.; Sherman, M. B.; Geissler, P. L.; Fletcher, D. A.; Hayden, C. C., Membrane bending by protein-protein crowding. *Nat. Cell Biol.* **2012,** *14* (9), 944-949.
11. Scheve, C. S.; Gonzales, P. A.; Momin, N.; Stachowiak, J. C., Steric pressure between membrane-bound proteins opposes lipid phase separation. *J. Am. Chem. Soc.* **2013,** *135* (4), 1185-1188.
12. Almeida, P. F., Thermodynamics of lipid interactions in complex bilayers. *Biochim. Biophys. Acta* **2009,** *1788* (1), 72-85.
13. Zeno, W. F.; Rystov, A.; Sasaki, D. Y.; Risbud, S. H.; Longo, M. L., Crowding-Induced Mixing Behavior of Lipid Bilayers: Examination of Mixing Energy, Phase, Packing Geometry, and Reversibility. *Langmuir : the ACS journal of surfaces and colloids* **2016,** *32* (18), 4688-4697.
14. Bricarello, D. A.; Smilowitz, J. T.; Zivkovic, A. M.; German, J. B.; Parikh, A. N., Reconstituted Lipoprotein: A Versatile Class of Biologically-Inspired Nanostructures. *ACS Nano* **2011,** *5* (1), 42-57.
15. Chromy, B. A.; Arroyo, E.; Blanchette, C. D.; Bench, G.; Benner, H.; Cappuccio, J. A.; Coleman, M. A.; Hoeprich, P. D., Different apolipoproteins impact nanolipoprotein particle formation. *J. Am. Chem. Soc.* **2007,** *129* (46), 14348-14354.
16. (a) Bayburt, T. H.; Sligar, S. G., Membrane protein assembly into Nanodiscs. *FEBS letters* **2010,** *584* (9), 1721-1727; (b) Denisov, I. G.; Grinkova, Y. V.; Lazarides, A. A.; Sligar, S. G., Directed Self-Assembly of Monodisperse Phospholipid Bilayer Nanodiscs with Controlled Size. *J. Am. Chem. Soc.* **2004,** *126* (11), 3477-3487.
17. Pack, D. W.; Chen, G.; Maloney, K. M.; Chen, C.-T.; Arnold, F. H., A metal-chelating lipid for 2D protein crystallization via coordination of surface histidines. *J. Am. Chem. Soc.* **1997,** *119* (10), 2479-2487.
18. (a) Zeno, W. F.; Hilt, S. L.; Aravagiri, K. A.; Risbud, S. H.; Voss, J. C.; Parikh, A. N.; Longo, M. L., Analysis of Lipid Phase Behavior and Protein Conformational Changes in Nanolipoprotein Particles upon Entrapment in Sol−Gel-Derived Silica. *Langmuir : the ACS journal of surfaces and colloids* **2014,** *30* (32), 9780-9788; (b) Zeno, W. F.; Hilt, S. L.; Risbud, S. H.; Voss, J. C.; Longo, M. L., Spectroscopic Characterization of Structural Changes in Membrane Scaffold Proteins Entrapped within Mesoporous Silica Gel Monoliths. *ACS Appl. Mater. Interfaces* **2015,** *7* (16), 8640-8649.
19. Israelachvili, J. N., *Intermolecular and surface forces: revised third edition*. Academic press: 2011.
20. (a) Ratto, T. V.; Longo, M. L., Obstructed diffusion in phase-separated supported lipid bilayers: a combined atomic force microscopy and fluorescence recovery after photobleaching approach. *Biophysical journal* **2002,** *83* (6), 3380-3392; (b) Przybylo, M.; Sýkora, J.; Humpolíčková, J.; Benda, A.; Zan, A.; Hof, M., Lipid diffusion in giant unilamellar vesicles is more than 2 times faster than in supported phospholipid bilayers under identical conditions. *Langmuir : the ACS journal of surfaces and colloids*

2006, *22* (22), 9096-9099; (c) Seu, K. J.; Pandey, A. P.; Haque, F.; Proctor, E. A.; Ribbe, A. E.; Hovis, J. S., Effect of surface treatment on diffusion and domain formation in supported lipid bilayers. *Biophysical journal* **2007,** *92* (7), 2445-2450.
21. Saffman, P.; Delbrück, M., Brownian motion in biological membranes. *Proceedings of the National Academy of Sciences* **1975,** *72* (8), 3111-3113.
22. Heberle, F. A.; Wu, J.; Goh, S. L.; Petruzielo, R. S.; Feigenson, G. W., Comparison of three ternary lipid bilayer mixtures: FRET and ESR reveal nanodomains. *Biophys. J.* **2010,** *99* (10), 3309-3318.

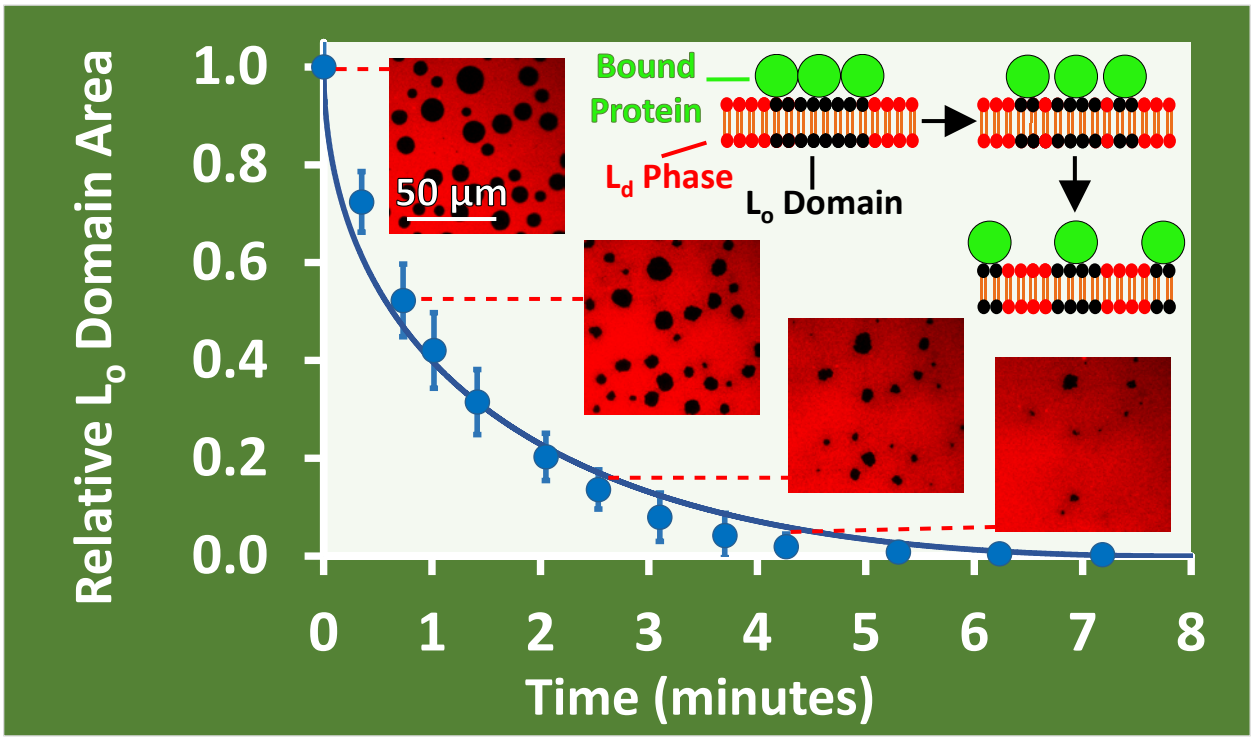

TOC Graphic